ACS OMEGA

http://pubs.acs.org/journal/acsodf

Article

NanoTafla Nanocomposite as a Novel Low-Cost and Eco-Friendly Sorbent for Strontium and Europium Ions

Elsayed M. Abu Elgoud, Mohamed I. Aly, Mostafa M. Hamed, and AbdElAziz A. Nayl*

Cite This: *ACS Omega* 2022, 7, 10447−10457

Read Online

ACCESS | Metrics & More | Article Recommendations | Supporting Information

ABSTRACT: Now the wide use of nanooxides is attributed to their remarkable collection of properties. Nanocomposites have an impressive variety of important applications. A thermal decomposition approach provides a more optimistic method for nanocrystal synthesis due to the low cost, high efficiency, and expectations for large-scale production. Therefore, in this study a new eco-friendly nanooxide composite with sorption characteristics for europium (Eu(III)) and strontium (Sr(II)) was synthesized by a one-step thermal treatment process using earth-abundant tafla clay as a starting material to prepare a modified tafla (M-Taf) nanocomposite. The synthesized nancomposite was characterized by different techniques before and after sorption processes. Different factors that affected the sorption behavior of Eu(III) and Sr(II) in aqueous media by the M-Taf nanocomposite were studied. The results obtained illustrated that the kinetics of sorption of Eu(III) and Sr(II) by the M-Taf nanocomposite are obeyed according to the pseudo-second order and controlled by a Langmuir isotherm model with maximum sorption capacities (Q_{max}) of 25.5 and 23.36 mg/g for Eu(III) and Sr(II), respectively. Also, this novel low-cost and eco-friendly sorbent has promising properties and can be used to separate and retain some radionuclides in different applications.

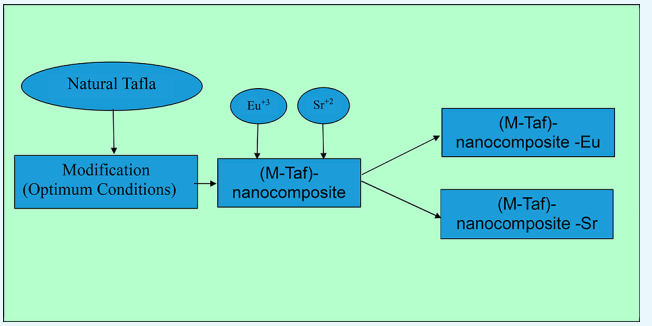

1. INTRODUCTION

During the last decades, as we've entered a new era of globalization, the purification and treatment of radioactive wastes became urgent demands to all countries before these wastes are discharged into the environment.[1,2] In the different nuclear industries, various types of massive radionuclides such as europium Eu(III) and strontium Sr(II) are generated, which can pollute the natural environment and seriously threaten living things.[2−6] Therefore, current efforts have been directed to reduce the risk of radiotoxicity of such radionuclides either before or after they are released into the environment, and we regard this as an issue of mounting concern due to the radioactivity and harmful impact on human health and aquatic environments.[7−11] The effective removal and efficient remediation of these radionuclides has become an urgent challenge in nuclear-waste management.[12−14] According to the International Energy Agency (IEA), by 2030 the capacities of the international nuclear industries will be developed by more than 40%, and this will promote the requirement of U^{6+} consumption and lead to the production of huge amounts of radioisotopes that might be released to the environment.[4] Strontium (^{90}Sr) and europium (^{152},^{154}Eu) are regarded as the main radionuclides in nuclear effluents and have severe biological toxicity including bone sarcoma, soft tissue cancer, arteriosclerosis diseases, rib bone and liver damages, leukemia, and endocrine system disruption.[15−17] Therefore, the removal of these radionuclides has acquired great attention and wide concern. So, a number of techniques, such as coagulation precipitation, extraction, filtration, precipitation, and adsorption, were applied to treat radioactive wastes and remove these radionuclides from aqueous solutions.[4,18−22] On the one hand, compared with various separation techniques and due to its advantages such as high selectivity, effectiveness, eco-friendly quality, and cost-effectiveness, sorption methods have been considered a quite promising technique,[15,16,23−25] where the sorbents reduce the radionuclide amount of large volumes of wastewater to a small volume of solid by different adsorption modes.[12] On the other hand, nanosorbents have various promising characteristics, like low cost, considerable surface area, porous structures, and low sorption equilibrium time, and therefore they are considered promising sorbents used to remove different types of radionuclides.[26,27] In recent decades, a variety of different sorbents and ion exchangers has been utilized to remove some radionuclides from wastewater. Clay minerals,[16,28−31] zeolites,[32−36] montmorillonite,[37,38] and carbonaceous materials (carbon nanotubes, graphene, and activated carbon)[39,40] are examples of these sorbents that have

Received: December 24, 2021
Accepted: March 3, 2022
Published: March 16, 2022

© 2022 The Authors. Published by American Chemical Society

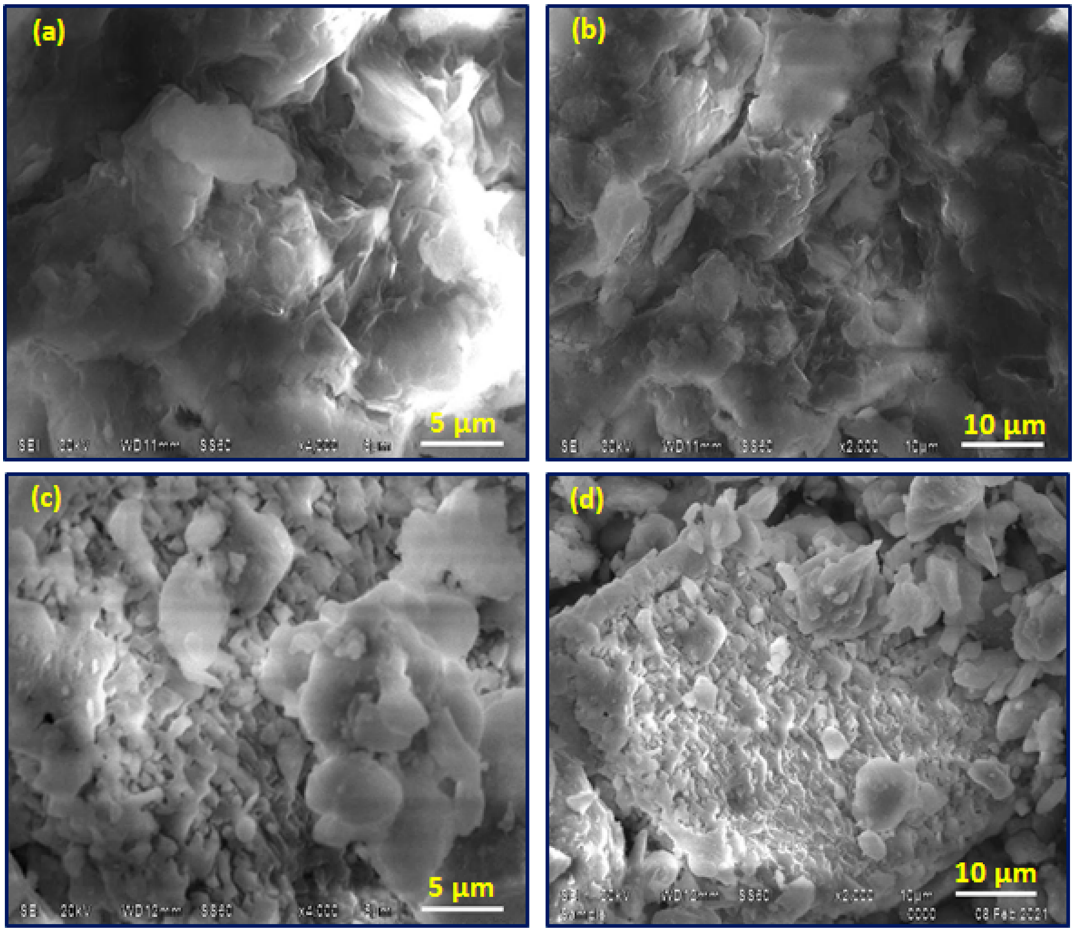

Figure 1. Images of SEM of the original tafla (a, b) and synthetic nanocomposite (c, d) with different magnification values.

attracted great attention during recent decades. The preparation of graphene oxide (GO)-based nanocomposites has been reported using the self-assembly of chitosan and graphene oxide and an in situ reduction approach.[41] Molybdenum compound nanoclusters supported on N-doped reduced graphene oxide have been prepared by carbonization and hydrothermal processes.[42,43] Also, poly(vinyl alcohol)/poly-(acrylic acid)/carboxylate graphene oxide nanosheet@polydopamine (PVA/PAA/GO−COOH@PDA) samples have been prepared by an electrospinning technique, thermal treatment, and polydopamine modification.[44]

Therefore, this work has been directed to prepare a novel nanoTaflanancomposite (M-Taf) as a low-cost and eco-friendly sorbent for strontium and europium species. The prepared nanocomposite was characterized by various techniques such as scanning electron microscopy (SEM), X-ray diffraction (XRD), transmission electron microscopy (TEM), and Fourier transform infrared (FTIR) spectroscopy. Various parameters, such as contact time, pH, volume-to-mass (V/m) ratio, initial metal ions concentration, and temperature, influenced the sorption processes, which were investigated.

2. EXPERIMENTAL SECTION

2.1. Chemicals and Materials. Herein, all the reagents and materials employed are of analytical grade and used as received without any further refining. Europium(III) nitratepentahydrate ($Eu(NO_3)_3{\cdot}5H_2O$), strontium chloridehexahydrate ($SrCl_2{\cdot}6H_2O$), nitric acid, and hydrochloric acid were supplied by Sigma-Aldrich, while NaOH was supplied by Adwic company for chemicals.

2.2. Synthesis of Nanocomposite. Tafla clay, which was used as a precursor for the nanooxides composite preparation, was collected from the Katameyya region, Cairo, Egypt. First, natural Tafla clay was crushed and washed several times with distilled water and stirred for several hours to remove impurities and other adhering materials. Then, the mixture was filtrated, and the filtrate was dried in the sunlight for 2.0 d. After it dried in the sunlight, the Tafla clay particles were sieved to obtain the particle size of 53 μm. The resulting Tafla powder was thermally treated in the muffle furnace (in an air atmosphere) by ramping the temperature (50 °C/10 min) until it reached 1000 °C, when it was held for 4 h. No other solvents or chemicals were used in the process of preparing this M-Taf nanoparticle.

The characterizations of the prepared modified Tafla (M-Taf nanocomposite) were achieved using a scanning electron microscope (JSM-6510A model), Fourier transmission infrared spectroscopy (Nicolet spectrometer). XRD measurements were made on a Shimadzu X-ray diffractometer obtained from Shimadzu Kyoto (model XD-Dl). The nanostructure of the M-Taf nanocomposite was inspected through a transmission electron microscope (JEM-2100). The chemical composition of the nanocomposite sample was analyzed by a PW-2400 Philips XRF spectrometer.

2.3. Batch Sorption Experiments. Batch adsorption experiments were done by shaking 0.05 g of new nanocomposite

https://doi.org/10.1021/acsomega.1c07255
ACS Omega 2022, 7, 10447−10457

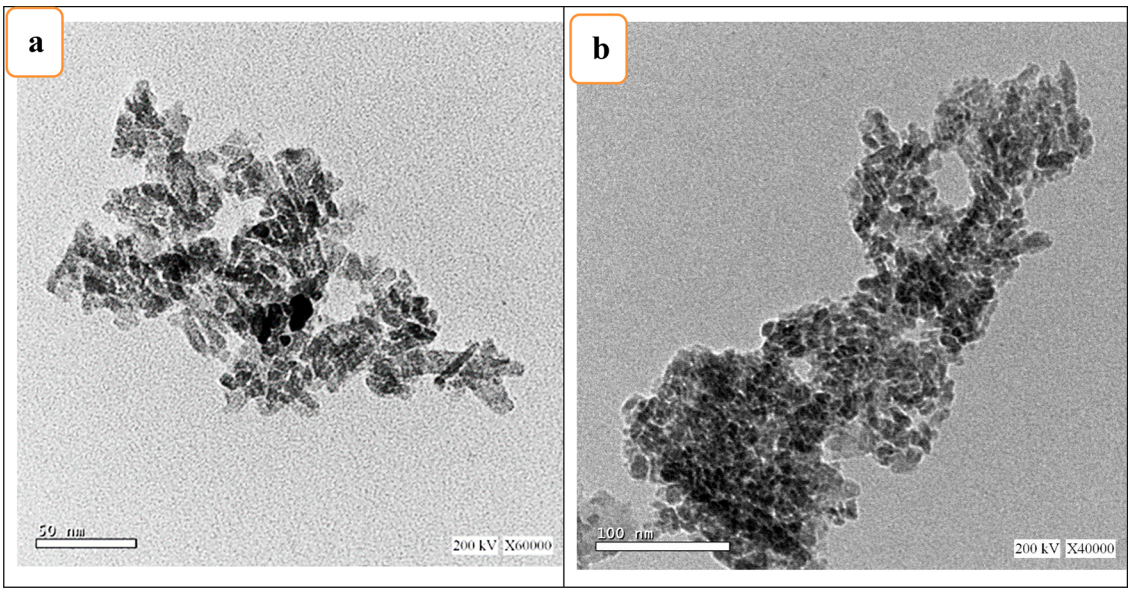

Figure 2. TEM images of prepared nanocomposite with magnification values of (a) X = 60 000 and (b) X= 40 000.

with 25.0 mL of 100 mg/L of Eu(III) and Sr(II) in a thermostated shaker bath (G.F.L. 1083) adjusted at 25 °C.

The concentration of Sr(II) was measured using an atomic absorption spectrophotometer, model S4 Series, Thermoelectron Corporation. The concentration of europium ions was determined spectrophotometrically by the Arsenazo-III method using a Shimadzu UV−visible double beam spectrophotometer model 160A. The pH measurements were performed by a Hanna pH meter with a resolution of 0.01 pH and accuracy of ±0.01.

Batch experiments were conducted to adsorb Eu(II) and Sr(II) from aqueous media onto the prepared nanocomposite at ambient temperature (25 °C ± 1). A 0.025 L solution of 100.0 mg/L for each investigated metal ion was mixed with 0.05 g of the new nanocomposite at the stirring rate of 400 rpm for 60.0 min at pH ≈ 5.0 for Eu(II) and 8.0 for Sr(II), unless otherwise cited.

In the sorption kinetics and isotherms, 0.05 g of the nanocomposite was transferred into a bottle containing 25.0 mL of a definite concentration of Eu(III) and Sr(II) ions. The mixture of nanocomposite and aqueous phases was mixed in a thermostated shaker bath for different time periods. The parameters affecting the sorption processes of Eu(III) and Sr(II) by a prepared nanocomposite were investigated and studied. The samples were withdrawn at certain times for analysis.

The percentage removal (%R) of Eu(III) and Sr(II) as well as the amount of metals ions sorbed at time t, q_t (mg/g), was calculated by

$$\%R = \frac{A_o - A_t}{A_o} \times 100 \quad (1)$$

$$q_t = \frac{A_o - A_t}{A_o} C_o \frac{V}{m} \quad (2)$$

where both A_o and A_t are the initial concentration and concentration at time t of $Eu^{3+}$and Sr^{2+} per unit volume, V (L) is the volume of the aqueous solution, while m (g) is the weight of the nanocomposite.

The thermodynamic parameters of the sorption processes, namely, $\Delta H°$, $\Delta S°$, and $\Delta G°$, were calculated by eqs 3−5).

$$K_d = \frac{q_e}{A_e} \quad (3)$$

$$\Delta G^o = -RT \ln k_d \quad (4)$$

$$\Delta G^o = \Delta H^o - T\Delta S^o \quad (5)$$

From Equation 5 in Equation 4

$$\ln k_d = \frac{\Delta S^o}{R} - \frac{\Delta H^o}{RT} \quad (6)$$

where ΔH^0, ΔS^0, ΔG^0, and K_d are the standard enthalpy, entropy, Gibbs free energy change, and the distribution coefficient (mL·g^{-1}), respectively, while R and T are the general gas constant (R = 8.314 J mol^{-1} K^{-1}) and absolute temperature (K), respectively. The relations between ln K_d against T^{-1} are linear. The slope of this relation gives the value of ΔH^0, and the intercept gives the value of ΔS^0.

2.4. Reusability Experiments. In this work, 100 mL of hot 5% HCl was utilized to desorb Eu(III) and Sr(II) from the prepared nanocomposite. The concentration of Eu(III) and Sr(II) in the desorption solution was measured spectrophotometrically, as shown above. %R of Eu(III) and Sr(II) was calculated using eq 1.

3. RESULTS AND DISCUSSION

3.1. Characterization of the Original Tafla and Prepared M-Tafnanocomposite. The chemical composition of the fabricated nanocomposite was analyzed by X-ray fluorescence (XRF) spectrometry. According to XRF analyses, the main chemical compositions are SiO_2 (62.911%), Al_2O_3 (13.9%), Fe_2O_3 (13.88), K_2O (2.48%), TiO_2 (2.72%), and other minor compositions. Most of these oxides have chemical and thermal stabilities under the investigated conditions.

The SEM images of original Tafla clay are represented in Figure 1 with different magnifications. Microstructures of the original particles demonstrated that the particles are composed of a highly crystalline form of sheets like polygonal flakes and are

https://doi.org/10.1021/acsomega.1c07255
ACS Omega 2022, 7, 10447−10457

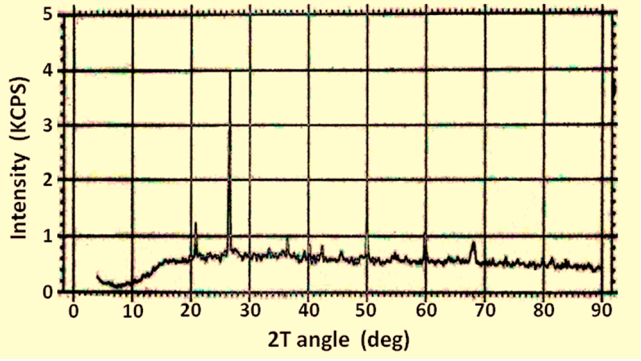

Figure 3. Crystal structure of prepared nanocomposite.

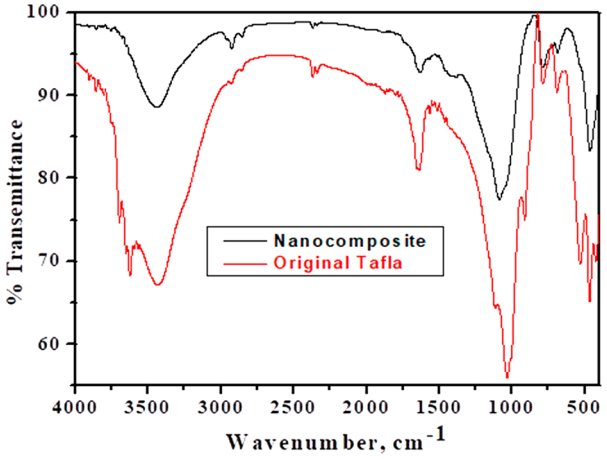

Figure 4. FTIR spectra of prepared nanocomposite and original Tafla.

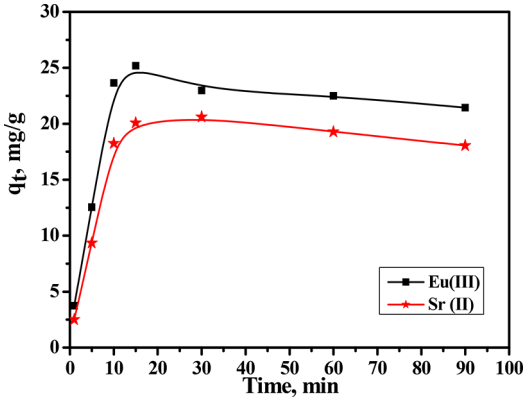

Figure 5. Effect of contact time on the removal of Eu(III) and Sr(II) by nanocomposite ([Eu] = 100.0 mg L^{-1}, pH_{Eu} = 5.0, [Sr] = 100.0 mg/L, pH_{Sr} = 8.0, ν = 0.025 L, dose = 0.05 g, T = 25 ± 1 °C).

structured to form the stacks.[45,46] Figure 1 also shows the surface morophology of the prepared nanocomposite at different magnifications. The micrograph of the prepared nanocomposite illustrates a vital change in the morophology structures compared with the original Tafla. The effect of the modification process on the Tafla samples shows that the surface area of the prepared nanocomposite has been increased due to the opening of the platelets, which also leads to a more porous characteristic in the nanocomposite structure.[47] The surface of the prepared nanocomposite has many advantages that enhance sorption processes such as irregularity, roughness, porosity, and heterogeneity.[48] These images indicate that the particles of the prepared nanocomposite have a polygonal shape. The successful formation of the new nanocomposite under the investigated conditions is confirmed by TEM and XRD analyses, as illustrated in Figures 2 and 3.

The data obtained by TEM measurements revealed the recognizable platy and hexagonal crystals of the prepared nanocomposite. These results emphasize the formation of structures obtained by the SEM analysis, Figure 1. Also, Figure 2 displays a propagation of a homogeneous morphology with conglomerate particles and relatively broad size distributions.[49]

The XRD pattern of the prepared M-Taf-nanocomposite is shown in Figure 3. The prominent bands at 20.9, 26.8, 33.4, 35.7, 41.9, 54.6, and 68.1 are characteristic bands that confirm the presence of a kaolinite mineral and quartz in the prepared nanocomposite.[45,50,51] The occurrence of more kaolinite approves the increase in the pore sizes of the prepared nanocomposite.[45]

The FTIR spectra of the prepared nanocomposite and the original Tafla were investigated and represented in Figure 4a,b to identify the function groups and to check for possible changes that could result from the modification processes.[52] For the original Tafla, Figure 4b, the absorption peaks observed at 3700 and 3400 cm^{-1} may be due to the stretching modes of Al−OH and the stretching vibrations of −OH in the tetrahedral and octahedral sheets of the original Tafla.[52,53] These peaks are changed and decreased for the prepared nanocomposite (Figure 4a) due to a dehydroxylation process.[54] Also, strong vibration bands detected at ∼1034 and 16 331 cm^{-1} may be due to the presence of O−Si−O, and these vibration bands are changed to appear at 1086, 1354, and 1432 cm^{-1} in the prepared nanocomposite due to surface chemistry changes that occur by a thermal activation.[53−55]

The vibration band at 913 cm^{-1} may be assigned to the presence of Al−O−H bending and inner hydroxyl groups. Also, absorption bands of Al−OH and Al−O−Si appear at ∼914, 961, and 531 cm^{-1}. The bands that appear in the range of 791−424 cm^{-1} are characteristic of Tafla and assigned to Si−O−Al or Si−O−Si vibrations.[53−55] In the prepared nanocomposite, the loss of −OH groups and Al−O−Si peaks approves the formation of amorphous SiO_2 and Al_2O_3 nanoparticles, and these are accompanied by the destruction of Al−O−Si bonds of the original Tafla.[55−57] Also, two main characteristic bands for the formation of silica nanoparticles appeared at ∼1086 and 791 cm^{-1} and are assigned to Si−O−Si peak vibration modes.[58,59]

3.2. Sorption Studies. *3.2.1. Influence of Contact Time.* The effect of contact time on the removal of Eu(III) and Sr(II) from aqueous solution using 0.05 g of nanocomposite was investigated as a function of mixing time in the range of 0.0−90 min using a batch adsorption experiment, and the results obtained are represented in Figure 5. The maximum removal percentage and equilibrium were reached for both Eu(III) and Sr(II), respectively. The results obtained reveal that the adsorption capacities of Eu(III) and Sr(II) by 0.05 g of nanocomposite increased rapidly by increasing the contact time within the first 15 min and then became slow to reach the equilibrium. This can be due to the large availability of the active sites on the nanocomposite. With further increase in time, there is almost no further increase in the sorption of both metals ions, and this can be due to fewer active sites being available on the nanocomposite.[56]

3.2.1.1. Adsorption Kinetic. In order to better understand the adsorption rates and pathway of the investigated sorption processes, the dynamics of adsorption processes of Eu(III) and

https://doi.org/10.1021/acsomega.1c07255
ACS Omega 2022, 7, 10447−10457

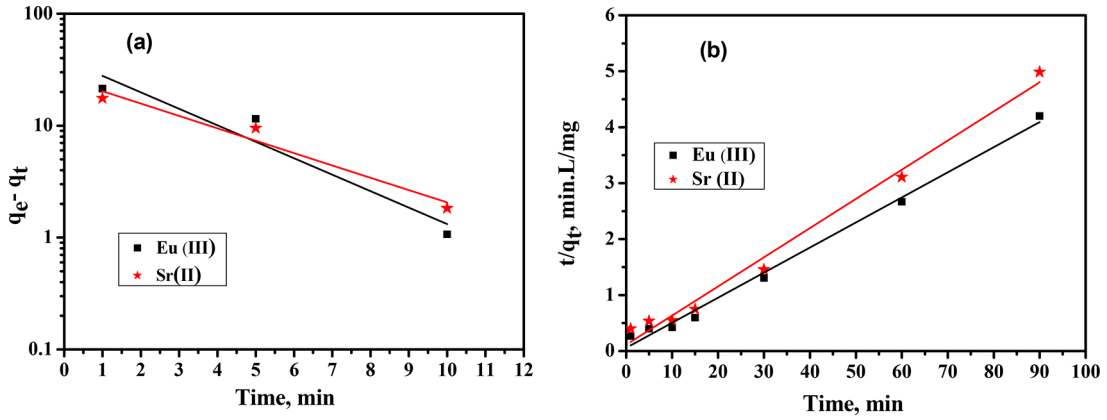

Figure 6. Adsorption kinetics of Eu(III) and Sr(II) ions with 0.05 g of nanocomposite. (a) Pseudo-first order and (b) pseudo-second order.

Table 1. Adsorption Kinetic Parameters[a] for the Adsorption of Eu(III) and Sr(II) Ions with 0.05 g of Nanocomposite at 298 K

	linear pseudo-first order		
metal ion	q_e calc mg/g	K_1, min^{-1}	R^2
Eu(III)	39.09	339.0×10^{-3}	0.866
Sr(II)	26.21	254.64×10^{-3}	0.925
	linear pseudo-second order		
	q_e calc mg/g	k_2, g/mg·min	R^2
Eu(III)	22.32	35.45×10^{-3}	0.992
Sr(II)	19.16	24.55×10^{-3}	0.986

[a]([Eu] = 100.0 mg/L, [Sr] = 100.0 mg/L, v = 0.025 L, dose = 0.05 g, Shaking time = 15.0 min, T = 25 ± 1 °C).

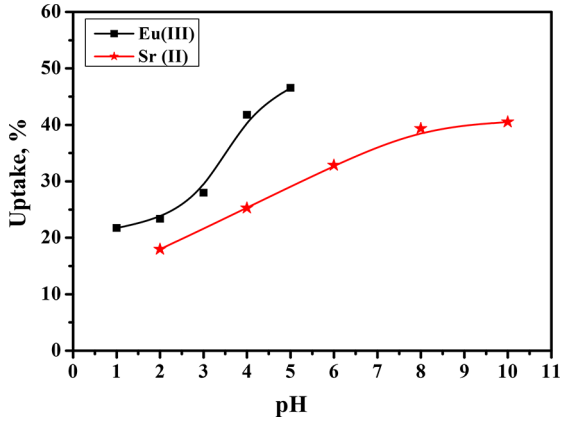

Figure 7. Effect of pH on the removal of Eu(III) and Sr(II) ions with 0.05 g of nanocomposite. ([Eu] = 100.0 mg L^{-1}, [Sr] = 100.0 mg/L, v = 0.025 L, dose = 0.05 g, shaking time = 15.0 min, T = 25 ± 1 °C)

Sr(II) by nanocompositeis were studied until an equilibrium reached.[61] Pseudo-first-order and pseudo-second-order processes were investigated and illustrated in Figure 6a,b, respectively, to analyze and calculate the rate constants and adsorption data, as in eqs 7 and 8.[15,26,60,61]

$$\log(q_e - q_t) = \log q_e + \frac{K_1 t}{2.303} \quad (7)$$

Here, q_e (mg·g^{-1}) and q_t (mg·g^{-1}) are the amounts of sorption at the equilibrium time and time t. k_1 (min^{-1}) is the rate constant of the pseudo-first-order sorption.

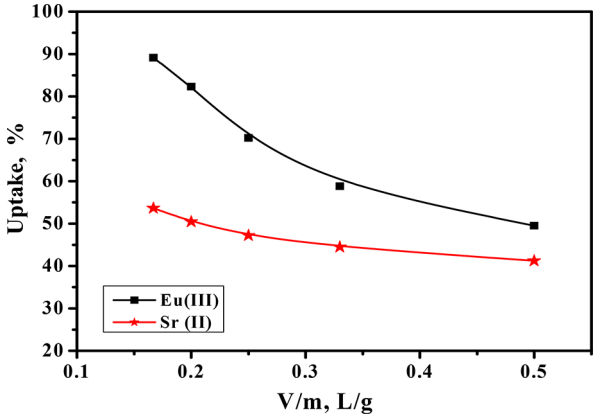

Figure 8. Effect of aqueous volume (V) on the adsorption of Eu(III) and Sr(II). [Eu] = 100.0 mg L^{-1}, pH_{Eu} = 5.0, [Sr] = 100.0 mg/L, pH_{Sr} = 8.0, shaking time = 15.0 min, T = 25 ± 1 °C.

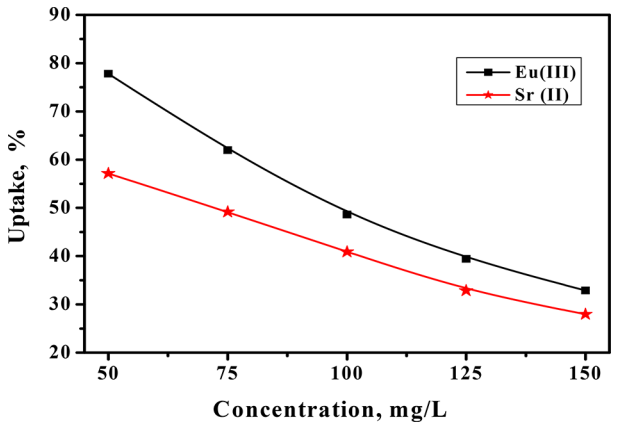

Figure 9. Effect of initial Eu(III) and Sr(II) concentrations on the adsorption rate by nanocomposite. [Eu] pH = 5.0, [Sr] pH = 8.0, v = 0.025 L, m = 0.05 g, shaking time = 15.0 min, T = 25 ± 1 °C.

$$\frac{t}{q} = \frac{1}{k_2 q_e^{\,2}} + \frac{1}{qe} t \quad (8)$$

K_2 (g mg^{-1} min^{-1}) is the rate constant of the pseudo-second-order sorption.

The kinetic parameters of the adsorption processes, such as q_{eexp}, k_1, q_{ecal}, R^2, and k_2, for a linear fitting of the experimental results are calculated from the intercept and slope of the plot represented in Figure 6a,b and illustrated in Table 1. The data

https://doi.org/10.1021/acsomega.1c07255
ACS Omega 2022, 7, 10447−10457

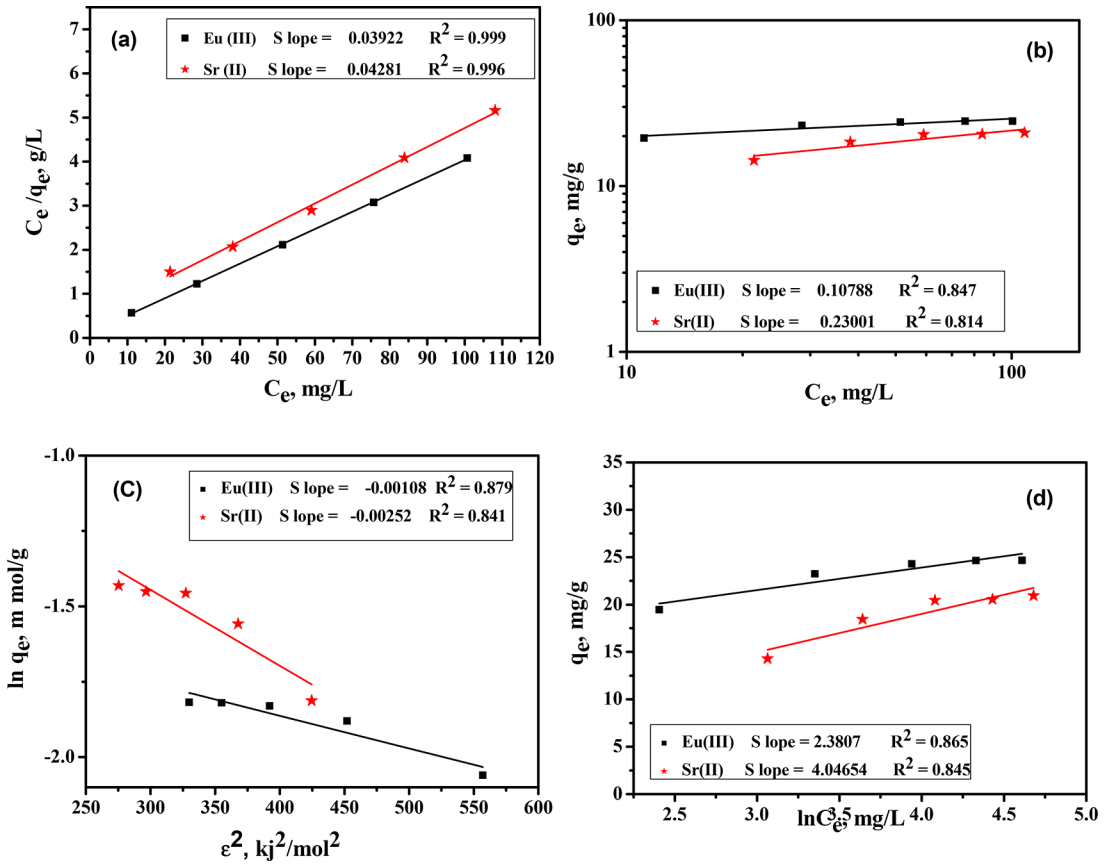

Figure 10. (a) Langmuir, (b) Freundlich, (C) Dubinin−Radushkevich, and (d) Temkin isotherm models for the adsorption of Eu(III) and Sr(II) by (M-Taf)-nanocomposite.

dissected that the Eu(III) and Sr(II) by nanocomposite shows an excellent fitting with the pseudo-second order ($R^2 \geq 0.992$ for Eu(III) and ≥0.986 for Sr(II)), indicating the sorption processes are a chemisorption process and agree well with the results reported in previous works.[12,15,26,58]

3.2.2. Influence of pH. The effect of pH (1.0−10) on the sorption of Eu(III) and Sr(II) by 0.05 g of nanocomposite was investigated at the optimum conditions, as shown in Figure 7, to examine how the metals ion sorption is strongly influenced by the initial pH of the solution.

The amounts of Eu(III) and Sr(II) adsorbed by nanocomposite were increased by increasing the pH values due to the electrostatic repulsion between positive charges on the nanocomposite and Eu(III) and Sr(II) ions.[26] The repulsion decreases with increased pH in this region and leads to an increase in the capacities values. At higher pH, sorption capacities of the nanocomposite rapidly reduce, which is due to the change in the charges on the surface of the nanocomposite.

All of these results may be explained depending on the fact that, at a low pH value, two mechanisms may be investigated to interpret the results. Here, the main Eu(III) species was Eu(III).[62,63] Here, the main species, namely, Eu(III), was at pH < 6.0.[12] Subsequently, the lower adsorption rate by the nanocomposite may be due to the competitive adsorption between Eu(III) ions and positively charged surface H^+/M^+ ions in ion exchange sites of the nanocomposite due to the electronic repulsion.[62] At higher pH, the dominant species of Eu(III) in the aqueous phase are Eu $(OH)_3$, $EuOH^{2+}$, and $Eu(OH)_2^+$, and therefore these species are sorbets in the higher pH range.[62] For Sr(II), as reported by Qi et al.,[64] Sr(II) is the prominent species when pH < 11.0. Therefore, the sorption rate is low at lower pH values, and it increased with further increase in the pH of media. With increases in the pH value of the solution, the surfaces of a nanocomposite become more negatively charged, and strong electrostatic interactions between Sr(II) with nanocomposite will form; therefore, the sorption capacities are enhanced, and more Sr(II) ions are removed.[65,66] This behavior may be due to weak acid cation exchange properties of the nanocomposite.[63]

3.2.3. Influence of V/m Ratio. The dependence of Eu(III) and Sr(II) removal on the *V*/*m* ratio (L/g) was investigated in the range as it was varied from 0.15 to 0.5 L/g by the nanocomposite. The data obtained, Figure 8, show that the rate of sorption first decreased rapidly with increases in the *V*/*m* ratio (L/g) until 0.35 g/L, and then it decreased slowly with further increases in the *V*/*m* ratio (L/g). This decrease in sorption efficiency is attributed to the fact that, with increases in the number of active sites on the nanocomposite surface, the ratio of these active sites to the number of sorbate ions is increased.[63]

3.2.4. Influence of Initial Metal Ion Concentrations. The effect of initial concentrations of Eu(III) and Sr(II) ions on the sorption processes by nanocomposite varying from 50 to 150 mg L^{-1} was studied, and the data obtained are represented in Figure 9. It is observed that, as the initial concentrations of Eu(III) and Sr(II) increase from 50 to 150 mg L^{-1}, the sorption capacity of Eu(III) and Sr(II) decreased from ∼80 to 40% for Eu(III) and from 58 to 38% for Sr(II), respectively. This may be explained by the fact that, with increases in the initial metal ion concentrations of Eu(III) and Sr(II), the available active sites

https://doi.org/10.1021/acsomega.1c07255
ACS Omega 2022, 7, 10447−10457

Table 2. Isotherm Parameters[a] for Adsorption Processes of Eu(III) and Sr(II) by Nanocomposite

		Freundlich parameters			Langmuir parameters			Dubinin–Radushkevic			Temkin			
metal ions	q_o, exp mg/g	K_f(mg/g)	n	R^2	Q_o (mg/g)	b (ml/mg)	R_L	R^2	q_m	β	R^2	E_{DR}	KT	bT	B	R^2
Eu(III)	24.66	15.5	9.27	0.847	25.5	0.337	0.029	0.999	0.239	0.0011	0.879	21.52	420.4	1040.56	2.38	0.865
Sr (II)	20.95	7.5	4.35	0.814	23.4	0.089	0.101	0.996	0.502	0.0025	0.841	14.09	2.0	612.20	4.05	0.845

[a][Eu] = 100.0 mg/L, pH_{Eu} = 5.0, [Sr] = 100.0 mg/L, pH_{Sr} = 8.0, m = 0.15 g, v = 0.025 L, shaking time = 15.0 min.

Table 3. Thermodynamic Parameters for Adsorption of Eu(III) and Sr(II) by Nanocomposite

metal ions	temp (K)	enthalpy change ($\Delta H°$), kJ mol^{-1}	entropy change ($\Delta S°$), J mol^{-1} K^{-1}	free energy change ($\Delta G°$), kJ mol^{-1}
Eu (III)	298	8.28	105.25	−23.08
	308			−24.14
	318			−25.19
	328			−26.24
	338			−27.29
Sr (II)	298	8.83	86.39	−16.91
	308			−17.78
	318			−18.64
	328			−19.51
	338			−20.37

in the surface of nanocomposite decreased, and saturation of the these sites occurred.

Therefore, the rates of adsorption of the studied cations were dropped.[65,67] The experimental data indicate that the affinity of the nanocomposite toward Eu(III) are higher than that for Sr(II).

3.2.5. Sorption Isotherm and Modeling. Different isotherm models are commonly used to evaluate the solid–liquid sorption systems.[26] Therefore, Langmuir, Freundlich, Dubinin–Radushkevich, and Temkin isotherm models are investigated and applied, as in eqs 9–15 to study the best fitting models, as presented in Figure 10a–d.

The Langmuir isotherm model has been applied extensively for dilute media and to describe the monolayer sorption processes, as in eq 9

$$\frac{C_e}{q_e} = \frac{1}{Q_{max} b} + \left[\frac{1}{Q_{max}}\right] C_e \tag{9}$$

where, C_e is the equilibrium concentration (mg L^{-1}) of the Eu(III) and Sr(II) ions, q_e is the Eu(III) and Sr(II) concentration (mg·g^{-1}) in the nanocomposite, and Q_{max} is the maximum monolayer sorption capacity (mg·g^{-1}) as represented in Figure 10a.

The Freundlich isotherm model supposes that the surface of a nanocomposite contains active sites that have several binding energies. The linearity equation is

$$\log q_e = \log K_f + \frac{1}{n} \log C_e \tag{10}$$

where K_f (mg·g^{-1}) and n are Freundlich constants that integrate the influence of all parameters, like the intensities of sorption and sorption capacities, on the sorption process. The Freundlich model considers the heterogeneity of a sorbent surface and the exponential distribution of active sites and their energy. For a favorable sorption, the values of n must be much greater than 1.0.

For many adsorption processes, the Dubinin–Radushkevich isotherm is more appropriate compared with the Freundlich mode, where it is not limited by constant sorption potential assumptions and homogeneous surfaces. It is represented by[64]

$$\ln q_e = \ln q_m - \beta\varepsilon^2 \tag{11}$$

where β is a constant related to the sorption energy and q_m the sorption capacity, and ε is the Polanyi potential and can be determined as in eq 12.

https://doi.org/10.1021/acsomega.1c07255
ACS Omega 2022, 7, 10447−10457

Table 4. Comparison of the Adsorption Behavior of Nanocomposite with with Different Sorbents Materials toward Eu(III) and Sr(II)

adsorbent	adsorption capacity (mg g^{-1}) (%R)[a]		equilibrium time, min	ref
	Eu^{3+}	Sr^{2+}		
MX-80 bentonite	46.06 (91.66%)	NR[b]	>30	62
polyacrylamide modified graphene oxide composites	NR[b]	2.11 mmol/g (93%)	360	64
Na-HEU zeolite	0.66 (mequiv/g) (87%)	NR[b]	240	69
"graphene oxide−magnetite" hybrid	NR[b]	14.3 (80%)	30	70
magnetic graphene oxides	NR[b]	14.706 (80%)	∼360	71
red clay	5.079(90%)	NR	720	72
dolomite powder	NR	1.172 (∼40%)	120	73
Sr-HAP	30.62(92.2%)	NR	∼1440	74
(Mg−Cd)HAP	30.91(93.6%)	NR	∼1440	74
NanoTaflaNanocomposite	25.5(89.15%)	23.36 (51.46%)	15	this study

[a]%R: removal percent. [b]NR: not reported.

$$\varepsilon = RT \ln [1 + (1/C_e)] \quad (12)$$

The mean free energy of sorption (E_{DR}) is determined from the β values by

$$E_{DR} = \frac{1}{\sqrt{2\beta}} \quad (13)$$

The Temkin isotherm model explains the interaction between sorbent and sorbate, as in eq 14

$$q_e = B_T \ln K_T + B_T \ln C_e \quad (14)$$

$$B_T = \frac{RT}{b} \quad (15)$$

where B_T (kJ·mol^{-1}) is the Temkin constant, which is related to the heat of adsorption, and k_T (L·mg^{-1}) is the equilibrium binding constant related to the maximum binding energies. The values of B_T and k_T may be calculated from the slopes and intercepts of straight lines of the plots of q_e versus ln C_e (Figure 10d).

The experimental results were fitted with the investigated isotherm models, Figure 10a−d, and their fitted factors and correlation coefficients (R^2) were calculated and represented in Table 2. The experimental results and calculations were well-represented by a Langmuir isotherm with R^2 values of 0.999 and 0.996 for Eu(III) and Sr(II), respectively, and with maximum adsorption capacities Q_e (mg/g) of 25.5 and 23.36 mg·g^{-1} for Eu(III) and Sr(II), respectively. Therefore, the adsorption processes of Eu(III) and Sr(II) using 0.05 g of nanocomposite are obedient to the Langmuir isotherm model. These results agree with those reported in previous works.[2,62,64,68]

Acoording to the calculated value of R^2 for the investigated isotherm models of the adsorption processes for Eu(III) and Sr(II) by nanocomposite, these adsorption processes obey the order Langmuir > Frendlich > Dubinin−Radushkevic > Temkin models.

3.2.6. Influence of Temperature and Thermodynamics Study. The influence of temperature on sorption processes has a considerable impact on the sorption capacities of the internal pores of sorbents and the diffusion rates of metal ions.[60] To calculate and evaluate the thermodynamic parameters of the investigated sorption processes, the influences of temperature on sorption capacity were studied (see Figure S1). The sorption rates of Eu(III) and Sr(II) by a nanocomposite at the optimum conditions are not affected or have an insignificant effect; increases in the temperature showed the stability of the bond between the metal ions and the surface of the prepared nanocomposite.

To understand the mechanisms involved in the investigated sorption processes of Eu(III) and Sr(II) by a nanocomposite at the optimum conditions under the effect of temperature, different thermodynamic parameters were calculated including ΔH^0, ΔS^0, and ΔG^0 from eqs 4−7 for the sorption systems under study.[60] As illustrated in Figure 10, the relationship between ln K_d and $1/T$ is linear, with the slope of $-\Delta H^0/R$ and the intercept of $\Delta S^\circ/R$, as illustrated in Figure S2. The values of thermodynamic parameters calculated by the linear relations are represented in Table 3. The positive values of ΔH^0 indicate an endothermic sorption process for both Eu(III) and Sr(II) by nanocomposite at the optimum conditions.

The positive values of ΔS^0 suggest the strong affinity of the nanocomposite toward both the metal ions during adsorption and high degree of randomness. It also indicates an increasing randomness in the adsorption systems and the irreversible processes that favor the complexation and stabilities of the adsorption systems.[45,60,64,67,68] The negative values of ΔG^0 imply that the sorption reactions are spontaneous and feasible at all the investigated temperatures.[67] It can be concluded that the sorption reactions of Eu(III) and Sr(II) onto a nanocomposite are endothermic and spontaneous processes, and these results agree with those reported before with various adsorbents.[45,60,64,67−71]

3.2.7. Reusability Study. The sorption−desorption reusability procedure was investigated using hot 5% HCl and repeated through five cycles. The data obtained illustrated that the sorption capacities of the prepared nanocomposite remained unchanged after five sorption/desorption runs. This is one of the most promising properties of the prepared Tafla-nanocomposite.

3.3. Comparison of the Sorption Behavior of (M-Taf)-Nanocomposite with Different Adsorbents toward Eu-(III) and Sr(II). The sorption capacities of the new nanocomposite toward Eu(III) and Sr(II) are compared with those of other various types of sorbents cited in the literature.[62,64,69−74] As reported in Table 4, the equilibrium times of adsorption processes of Eu(III) and Sr(II) onto nanocomposite are faster than that for the other adsorbents. In our work the equilibrium is faster and reached at ∼15 min for both Eu(III) and Sr(II), while the least equilibrium times reported by other works were reached at ∼30 min for Eu(III)[62] and Sr(II).[70]

Also the nanocomposite has considerable sorption capacities for both Eu(III) and Sr(II) compared with other materials, as in

https://doi.org/10.1021/acsomega.1c07255
ACS Omega 2022, 7, 10447−10457

Table 4. Therefore, nanocomposite can be considered as an eco-friendly and promising nanomaterial utilized to separate and remove such metal ions from different wastes.

4. CONCLUSION

A novel nanoTafla nancomposite was prepared as a low-cost and eco-friendly sorbent for strontium and europium ions from aqueous media. Under the optimum conditions, the investigated sorption processes suggest the strong affinity of nanocomposite toward both Eu(III) and Sr(II). The data obtained show an endothermic and spontaneous characteristic that is feasible at all the investigated temperatures at the optimum conditions with increases in the randomness of the processes and is obedient to the pseudo-second order. The sorption processes are pH-controlled and fitted with Langmuir isotherm models. Therefore, this promising nanocomposite can be used to separate and retain radionuclides in different applications.

■ ASSOCIATED CONTENT

Supporting Information

The Supporting Information is available free of charge at https://pubs.acs.org/doi/10.1021/acsomega.1c07255.

Effect of temperature on adsorption of Eu(III) and Sr(II) by (M-Taf)-nanocomposite; relationship between ln K_d and $1/T$ for the adsorption of Eu(III) and Sr(II) by (M-Taf)-nanocomposite (PDF)

■ AUTHOR INFORMATION

Corresponding Author

AbdElAziz A. Nayl − *Department of Chemistry, College of Science, Jouf University, Sakaka 42421 Aljouf, Saudi Arabia;* orcid.org/0000-0003-0531-5194; Email: aanayel@ju.edu.sa, aanayl@yahoo.com

Authors

Elsayed M. Abu Elgoud − *Hot Laboratories and Waste Management Center, Egyptian Atomic Energy Authority, Cairo 13759, Egypt*

Mohamed I. Aly − *Hot Laboratories and Waste Management Center, Egyptian Atomic Energy Authority, Cairo 13759, Egypt;* orcid.org/0000-0001-9903-0151

Mostafa M. Hamed − *Hot Laboratories and Waste Management Center, Egyptian Atomic Energy Authority, Cairo 13759, Egypt*

Complete contact information is available at: https://pubs.acs.org/10.1021/acsomega.1c07255

Notes

The authors declare no competing financial interest.

■ ACKNOWLEDGMENTS

We acknowledge the financial support from Egyptian Atomic Energy Authority.

■ REFERENCES

(1) Huang, Z.-W.; Li, Z.-J.; Zheng, L. R.; Wu, W.-S.; Chai, Z. F.; Shi, W. Q. Adsorption of Eu(III) and Th(IV) on three-dimensional graphene-based macrostructure studied by spectroscopic investigation. *Environ. Pollut.* **2019**, *248*, 82−89.

(2) Shin, J.; Lee, Y. G.; Kwak, J.; Kim, S.; Lee, S.-H.; Park, Y.; Lee, S.-D.; Chon, K. Adsorption of radioactive strontium by pristine and magnetic biochars derived from spent coffee grounds. *J. Environ. Chem. Eng.* **2021**, *9*, 105119.

(3) Chen, C.; Yang, X.; Wei, J.; Tan, X.; Wang, X. Eu(III) uptake on rectorite in the presence of humic acid: A macroscopic and spectroscopic study. *J. Colloid Interface Sci.* **2013**, *393*, 249−256.

(4) Wang, X.; Chen, L.; Wang, L.; Fan, Q.; Pan, D.; Li, J.; Chi, F.; Xie, Y.; Yu, S.; Xiao, C.; Luo, F.; Wang, J.; Wang, X.; Chen, C.; Wu, W.; Shi, W.; Wang, S.; Wang, X. Synthesis of novel nanomaterials and their application in efficient removal of radionuclides. *Sci. China: Chem.* **2019**, *62*, 933−967.

(5) Wu, Y.; Pang, H.; Liu, Y.; Wang, X.; Yu, S.; Fu, D.; Chen, J.; Wang, X. Environmental remediation of heavy metal ions by novel-nanomaterials: A review. *Environ. Pollut.* **2019**, *246*, 608−620.

(6) Yu, S.; Yin, L.; Pang, H.; Wu, Y.; Wang, X.; Zhang, P.; Hu, B.; Chen, Z.; Wang, X. Constructing sphere-like cobalt-molybdenum-nickel ternary hydroxide and calcined ternary oxide nanocomposites for efficient removal of U(VI) from aqueous solutions. *Chem. Eng. J.* **2018**, *352*, 360−370.

(7) Zhang, R.; Chen, C.; Li, J.; Wang, X. Preparation of montmorillonite@carbon composite and its application for U(VI) removal from aqueous solution. *Appl. Surf. Sci.* **2015**, *349*, 129−137.

(8) Wang, L.; Tao, W.; Yuan, L.; Liu, Z.; Huang, Q.; Chai, Z.; Gibson, J. K.; Shi, W. Rational control of the interlayer space inside two-dimensional titanium carbides for highly efficient uranium removal and imprisonment. *Chem. Commun.* **2017**, *53*, 12084−12087.

(9) Missana, T.; Garcıa-Gutierrez, M. Adsorption of bivalent ions (Ca(II), Sr(II) and Co(II)) onto FEBEX bentonite. *Phys. Chem. Earth* **2007**, *32*, 559−567.

(10) Veliscek-Carolan, J. Separation of actinides from spent nuclear fuel: A review. *J. Hazard. Mater.* **2016**, *318*, 266−281.

(11) Fryxell, G. E.; Mattigod, S. V.; Lin, Y. H.; Wu, H.; Fiskum, S.; Parker, K.; Zheng, F.; Yantasee, W.; Zemanian, T. S.; Addleman, R. S.; Liu, J.; Kemner, K.; Kelly, S.; Feng, X. D. Design and synthesis of self-assembled monolayers on mesoporous supports (SAMMS): the importance of ligand posture in functional nanomaterials. *J. Mater. Chem.* **2007**, *17*, 2863−2874.

(12) Zhang, P.; Wang, L.; Yuan, L.-Y.; Lan, J.-H.; Chai, Z.-F.; Shi, W.-Q Sorption of Eu(III) on MXene-derived titanate structures: The effect of nanoconfined space. *Chem. Eng. J.* **2019**, *370*, 1200−1209.

(13) Huang, Z. W.; Li, Z. J.; Wu, Q.-Y.; Zheng, L.-R.; Zhou, L.-M.; Chai, Z.-F.; Wang, X.-L.; Shi, W.-Q. Simultaneous elimination of cationic uranium(vi) and anionic rhenium (vii) by graphene oxide−poly(ethyleneimine) macrostructures: a batch, XPS, EXAFS, and DFT combined study. *Environ. Sci.: Nano* **2018**, *5*, 2077−2087.

(14) Zhang, P.; Wang, L.; Du, K.; Wang, S.; Huang, Z.; Yuan, L.; Li, Z.; Wang, H.; Zheng, L.; Chai, Z.; Shi, W. Effective removal of U(VI) and Eu(III) by carboxyl functionalized MXenenanosheets. *J. Hazard. Mater.* **2020**, *396*, 122731.

(15) Wang, S.; Ning, S.; Zhang, W.; Zhang, S.; Zhou, J.; Wang, X.; Wei, Y. Synthesis of carboxyl group functionalized silica composite resin for strontium removal. *Mater. Des* **2020**, *185*, 108224.

(16) Xiang-Xue, W.; Shu-Jun, Y. U.; Xiang-Ke, W. Removal of radionuclides by metal-organic framework-based materials. *J. Inorg. Mater.* **2019**, *34*, 17.

(17) Migaszewski, Z. M.; Gałuszka, A. The characteristics, occurrence, and geochemical behavior of rare earth elements in the environment: A review, Critic. Rev. *Environ. Sci. Technol.* **2015**, *45*, 429−471.

(18) De Jesus, K.; Rodriguez, R.; Baek, D. L.; Fox, R. V.; Pashikanti, S.; Sharma, K. Extraction of lanthanides and actinides present in spent nuclear fuel partitioning and in electronic waste. *J. Mol. Liq.* **2021**, *336*, 116006.

(19) Johnson, B. E.; Santschi, P. H.; Chuang, C. Y.; Otosaka, S.; Addleman, R. S.; Douglas, M.; Rutledge, R. D.; Chouyyok, W.; Davidson, J. D.; Fryxell, G. F.; Schwantes, J. M. Collection of lanthanides and actinides from natural waters with conventional and nanoporous sorbents. *Environ. Sci. Technol.* **2012**, *46*, 11251−11258.

(20) Manos, M. J.; Kanatzidis, M. G. Metal sulfide ion exchangers: superior sorbents for the capture of toxic and nuclear waste-related metal ions. *Chem. Sci.* **2016**, *7*, 4804−4824.

(21) Panak, P. J.; Geist, A. Complexation and extraction of trivalent actinides and lanthanides by triazinylpyridine N-donor ligands. *Chem. Rev.* **2013**, *113*, 1199−1236.
(22) Yin, L.; Song, S.; Wang, X. X.; Niu, F. L.; Ma, R.; Yu, S. J.; Wen, T.; Chen, Y. T.; Hayat, T.; Alsaedi, A.; Wang, X. K. Rationally designed core-shell and yolk-shell magnetic titanatenanosheets for efficient U(VI) adsorption performance. *Environ. Pollut.* **2018**, *238*, 725−738.
(23) Qi, X.-H.; Du, K.-Z.; Feng, M.-L.; Gao, Y.-J.; Huang, X.-Y.; Kanatzidis, M. G. Layered $A_2Sn_3S_7{\cdot}1.25H_2O$ (A = Organic Cation) as efficient ion-exchanger for rare earth element recovery. *J. Am. Chem. Soc.* **2017**, *139*, 4314−4317.
(24) Wang, X.; Chen, L.; Wang, L.; Fan, Q.; Pan, D.; Li, J.; Chi, F.; Xie, Y.-I.; Yu, S.; Xiao, C.; Luo, F.; Wang, J.; Wang, X.; Chen, C.; Wu, W.; Shi, W.; Wang, S.; Wang, X. Synthesis of novel nanomaterials and their application in efficient removal of radionuclides. *Sci. China: Chem.* **2019**, *62*, 933−967.
(25) Xiang-Xue, W.; Shu-Jun, Y.; Xiang-Ke, W. Removal of radionuclides by metal-organic framework-based materials. *J. Inorg. Mater.* **2019**, *34*, 17.
(26) Zahran, F.; El-Maghrabi, H. H.; Hussein, G.; Abdelmaged, S. M. Fabrication of bentonite based nanocomposite as a novel low cost adsorbent for uranium ion removal. *Environ. Nanotechnol. Monit. Manage* **2019**, *11*, 100205.
(27) Kyzas, G. Z.; Matis, K. A. Nanoadsorbents for pollutants removal: a review. *J. Mol. Liq.* **2015**, *203*, 159−168.
(28) Rabung, T.; Pierret, M. C.; Bauer, A.; Geckeis, H.; Bradbury, M. H.; Baeyens, B. Sorption of Eu(III)/Cm(III) on Ca-montmorillonite and Na-Illite. Part 1: Batch sorption and time-resolved laser fluorescence spectroscopy experiments. *Geochim. Cosmochim. Acta* **2005**, *69*, 5393−5402.
(29) Galunin, E.; Alba, M. D.; Santos, M. J.; Abrao, T.; Vidal, M. Lanthanide sorption on smectitic clays in presence of cement leachates. *Geochim. Cosmochim. Acta* **2010**, *74*, 862−875.
(30) Li, T.; Huang, X.; Wang, Q.; Yang, G. Adsorption of metal ions at kaolinite surfaces: Ion-specific effects, and impacts of charge source and hydroxide formation. *Appl. Clay Sci.* **2020**, *194*, 105706.
(31) Uddin, M. K. A review on the adsorption of heavy metals by clay minerals, with special focus on the past decade. *Chem. Eng. J.* **2017**, *308*, 438−462.
(32) Sun, Y.; Li, J.; Wang, X. The retention of uranium and europium onto sepiolite investigated by macroscopic, spectroscopic and modeling techniques. *Geochim. Cosmochim. Acta* **2014**, *140*, 621−643.
(33) Noli, F.; Kapnisti, M.; Buema, G.; Harja, M. Retention of barium and europium radionuclides from aqueous solutions on ash-based sorbents by application of radiochemical techniques. *Appl. Radiat. Isot.* **2016**, *116*, 102−109.
(34) Kallo, D. N. Applications of natural zeolites in water and wastewater treatment. *Rev. Mineral. Geochem* **2001**, *45*, 519−550.
(35) Rhodes, C. I. Properties and applications of zeolites. *Sci. Prog.* **2010**, *93*, 223−284.
(36) Lee, H. Y.; Kim, H. S.; Jeong, H.-K.; Park, M.; Chung, D.-Y.; Lee, K.-Y.; Lee, E. H.; Lim, W. T. Selective removal of radioactive cesium from nuclear waste by zeolites: on the origin of cesium selectivity revealed by systematic crystallographic studies. *J. Phys. Chem. C* **2017**, *C121*, 10594−10608.
(37) Wang, Y.-Q.; Zheng, Z.-Y.; Zhao, Y.-K.; Huang, J. H.; Zhang, Z.-B.; Cao, X.-H.; Dai, Y.; Hua, R.; Liu, Y.-H. Adsorption of U(VI) on montmorillonite pillared with hydroxyaluminum. *J. Radioanal. Nucl. Chem.* **2018**, *317*, 69−80.
(38) Xin, Y.; Wang, J.; Li, Y.; Asiri, A. M.; Marwani, H. M.; Hu, S.; Wang, G.; Xu, Z. Influence of humic acid on the immobilization of U(VI) by montmorillonite in simulated environmental conditions. *Sep. Sci. Technol.* **2018**, *53*, 696−706.
(39) Fan, Q. H.; Shao, D. D.; Hu, J.; Chen, C. L.; Wu, W. S.; Wang, X. K. Adsorption of humic acid and Eu(III) to multi-walled carbon nanotubes: Effect of pH, ionic strength and counterion effect. *Radiochim. Acta* **2009**, *97*, 141−148.
(40) Gad, H. M. H.; Awwad, N. S. Factors affecting on the sorption/desorption of Eu (III) using activated carbon. *Sep. Sci. Technol.* **2007**, *42*, 3657−3680.
(41) Zhao, H.; Jiao, T.; Zhang, L.; Zhou, J.; Zhang, Q.; Peng, Q.; Yan, X. Preparation and adsorption capacity evaluation of graphene oxide-chitosan composite hydrogels. *Sci. China: Chem.* **2015**, *58*, 811−818, DOI: 10.1007/s40843-015-0090-x.
(42) Xing, R.; Wang, W.; Jiao, T.; Ma, K.; Zhang, Q.; Hong, W.; Qiu, H.; Zhou, J.; Zhang, L.; Peng, Q. BioinspiredPolydopamine Sheathed Nanofibers Containing Carboxylate Graphene Oxide Nanosheet for High-Efficient Dyes Scavenger. *ACS Sustainable Chem. Eng.* **2017**, *5*, 4948−4956.
(43) Xu, Y.; Wang, R.; Wang, J.; Li, J.; Jiao, T.; Liu, Z. Facile fabrication of molybdenum compounds (Mo_2C, MoP and MoS_2) nanoclusters supported on N-doped reduced graphene oxide for highly efficient hydrogen evolution reaction over broad pH range. *Chem. Eng. J.* **2021**, *417*, 129233.
(44) Cui, Y.; He, H.; Atkinson, J. D. Iron/Carbon Composites for Cr(VI) Removal Prepared from HarmfulAlgal Bloom Biomass via Metal Bioaccumulation or Biosorption. *ACS Sustainable Chem. Eng.* **2019**, *7*, 1279−1288.
(45) Dim, P. E.; Mustapha, L. S.; Termtanun, M.; Okafor, J. O. Adsorption of chromium (VI) and iron (III) ions onto acid-modified kaolinite: Isotherm, kinetics and thermodynamics studies. *Arabian J. Chem.* **2021**, *14*, 103064.
(46) Mudzielwana, R.; Gitari, W. M.; Msagati, T. A. M. Characterisation of smectite rich clay soils: implication for groundwater defluoridation. *S. Afr. J. Sci.* **2016**, *112*, 1−8.
(47) Abukhadra, M. R.; AlHammadi, A.; El-Sherbeeny, A. M.; Salam, M. A.; El-Meligy, M. A.; Awwad, E. M.; Luqman, M. Enhancing the removal of organic and inorganic selenium ions using an exfoliated kaolinite/cellulose fibresnanocomposite. *Carbohydr. Polym.* **2021**, *252*, 117163.
(48) Sternik, D.; Galaburda, M. V.; Bogatyrov, V. M.; Oranska, O. I.; Charmas, B.; Gun'ko, V. M. Novel porous carbon/clay nanocomposites derived from kaolinite/ resorcinol-formaldehyde polymer blends: synthesis, structure and sorption properties. *Appl. Surf. Sci.* **2020**, *525*, 146361.
(49) Tchanang, G.; Djangang, C. N.; Abi, C. F.; Moukouri, D. L. M.; Blanchart, P. Synthesis of reactive silica from kaolinitic clay: Effect of process parameters. *Appl. Clay Sci.* **2021**, *207*, 106087.
(50) Zhong, M.; Zou, D.; Xu, Y.; Jin, L.; Pan, Y. Effect of kaolinites modified with Zr and transition metals on the pyrolysis behaviors of low-rank coal and its model compound. *J. Energy Inst* **2021**, *95*, 41−51.
(51) Nasrollahzadeh, M.; Shafiei, N.; Baran, T.; Pakzad, K.; Tahsili, M. R.; Baran, N. Y.; Shokouhimehr, M. Facile synthesis of Pd nanoparticles supported on a novel Schiffbase modified chitosan-kaolin: Antibacterial and catalytic activities in Sonogashira coupling reaction. *J. Organomet. Chem.* **2021**, *945*, 121849.
(52) Fei, F.; Gao, Z.; Wu, H.; Wurendaodi, W.; Zhao, S.; Asuha, S. Facile solid-state synthesis of Fe_3O_4/kaolinite nanocomposites for enhanced dye adsorption. *J. Solid State Chem.* **2020**, *291*, 121655.
(53) Masanje Malima, N.; John Owonubi, S.; Hellen Lugwisha, E.; Simon Mwakaboko, A. Development of cost-effective and eco-friendly adsorbent by direct physical activation of Tanzanian Malangali kaolinite for efficient removal of heavy metals. *Mater. Today: Proc.* **2021**, *38*, 1126−1132.
(54) Olusegun, S. J.; Mohallem, N. D. S. Comparative adsorption mechanism of doxycycline and Congo red using synthesized kaolinite supported $CoFe_2O_4$ nanoparticles. *Environ. Pollut.* **2020**, *260*, 114019.
(55) Behnamfard, A.; Chegni, K.; Alaei, R.; Vegliò, F. The effect of thermal and acid treatment of kaolin on its ability for cyanide removal from aqueous solutions. *Environ. Earth. Sci.* **2019**, *78*, 408.
(56) Wei, Y.; Yuan, P.; Song, Y.; Liu, D.; Losic, D.; Tan, D.; Chen, F.; Liu, H.; Du, P.; Zhou, J. Activating 2D nano-kaolinite using hybrid nanoparticles for enhanced phosphate capture. *Chem. Commun.* **2018**, *54*, 11649−11652.
(57) Liu, X.; Liu, X.; Hu, Y. Investigation of the thermal behaviour and decomposition kinetics of kaolinite. *Clay Miner* **2015**, *50*, 199−209.

https://doi.org/10.1021/acsomega.1c07255
ACS Omega 2022, 7, 10447−10457

(58) Patel, B.; Patel, P. Synthesis and characterization of silica nanoparticles by acid leaching technique. *Res. J. Chem. Sci.* **2014**, *4*, 52−55.
(59) Xu, D.; Chen, W.; Luo, Y.; et al. Amorphous TiO_2 layer on silicon monoxide nanoparticles as stable and scalable core-shell anode materials for high performance lithium ion batteries. *Appl. Surf. Sci.* **2019**, *479*, 980−988.
(60) Mustapha, S.; Tijani, J. O.; Ndamitso, M. M.; Abdulkareem, A. S.; Shuaib, D. T.; Mohammed, A. K. Adsorptive removal of pollutants from industrial wastewater using mesoporous kaolin and kaolin/TiO_2nanoadsorbents. *Environ. Nanotechnol. Monit. Manage* **2021**, *15*, 100414.
(61) Zeng, X.; Liu, Y.; Zhang, T.; Jin, J.-C.; Li, J.-L.; Sun, Q.; Ai, Y.-J.; Feng, M.-L.; Huang, X.-Y. Ultrafast and selective uptake of Eu^{3+} from aqueous solutions by two layered sulfides. *Chem. Eng. J.* **2021**, *420*, 127613.
(62) He, Y.; Chen, Y.-G.; Ye, W.-M.; Zhang, X.-X. Effects of contact time, pH, and temperature on Eu(III) sorption onto MX-80 bentonite. *Chem. Phys.* **2020**, *534*, 110742.
(63) Chen, C.; Hu, J.; Xu, D.; Tan, X.; Meng, Y.; Wang, X. Surface complexation modeling of Sr(II) and Eu(III) adsorption onto oxidized multiwall carbon nanotubes. *J. Colloid Interface Sci.* **2008**, *323*, 33−41.
(64) Qi, H.; Liu, H.; Gao, Y. Removal of Sr(II) fromaqueous solutions using polyacrylamidemodifiedgraphene oxide composites. *J. Mol. Liq.* **2015**, *208*, 394−401.
(65) Hamed, M. M.; Shahr El-Din, A. M.; Abdel-Galil, E. A. Nanocomposite of polyaniline functionalized Tafla: synthesis, characterization, and application as a novel sorbent for selective removal of Fe(III). *J. Radioanal. Nucl. Chem.* **2019**, *322*, 663−676.
(66) Zhao, G. X.; Li, J. X.; Ren, X. M.; Chen, C. L.; Wang, X. K. Few-layered graphene oxide nanosheets as superior sorbents for heavy metal ion pollution management. *Environ. Sci. Technol.* **2011**, *45*, 10454−10462.
(67) Liu, H.; Xiong, Z.; Peng, R.; Gong, B.; Chang, L.; Yang, J.; Zhao, Y.; Zhang, J. Elemental mercury removal from simulated coal-fired flue gas by modified tonstein in coal seam. *Fuel* **2021**, *284*, 119016.
(68) Sun, Z.; Chen, Y.-G.; Cui, Y.-J.; Ye, W.-M. Adsorption of Eu(III) onto Gaomiaozibentonite corroded by cement waters: Effect of cement solutions on the long-term sorption performance of bentonite in the repository conditions. *J. Cleaner Prod* **2020**, *251*, 119692.
(69) Sharma, P.; Sharma, M.; Tomar, R. Na-HEU zeolite synthesis for the removal of Th(IV) and Eu(III) from aqueous waste by batch process. *J. Taiwan Inst. Chem. Eng.* **2013**, *44*, 480−488.
(70) Tayyebi, A.; Outokesh, M.; Moradi, A.; Doram, A. Synthesis and characterization of ultrasound assisted "grapheneoxide−magnetite" hybrid, and investigation of its adsorptionproperties for Sr(II) and Co(II) ions. *Appl. Surf. Sci.* **2015**, *353*, 350−362.
(71) Li, D.; Zhang, B.; Xuan, E. The sequestration of Sr(II) and Cs(I) from aqueous solutions bymagneticgraphene oxides. *J. Mol. Liq.* **2015**, *209*, 508−514.
(72) Yu, T.; Wu, W. S.; Liu, Z.; Zhang, S. W.; Nie, Z. W. Kinetic and thermodynamic study of Eu(III) sorption on natural red earth in South China. *Korean J. Chem. Eng.* **2013**, *30*, 440−447.
(73) Ghaemi, A.; Torab-Mostaedi, M.; Ghannadi-Maragheh, M. Characterizations of strontium(II) and barium(II) adsorption from aqueous solutions using dolomite powder. *J. Hazard. Mater.* **2011**, *190*, 916−921.
(74) Sheha, R. R.; Moussa, S. I.; Attia, M. A.; Sadeek, S. A.; Someda, H. H. Novel substituted Hydroxyapatite nanoparticles as a solid phase for removal of Co(II) and Eu(III) ions from aqueous solutions. *J. Environ. Chem. Eng.* **2016**, *4*, 4808−4816.

https://doi.org/10.1021/acsomega.1c07255
ACS Omega 2022, 7, 10447−10457